

Solvation dynamics in dielectric solvents with restricted molecular rotations: Polyethers

Roberto Olender

Department of Chemical Physics, The Weizmann Institute of Science, Rehovot 76100, Israel

Abraham Nitzan

School of Chemistry, The Sackler Faculty of Science, Tel Aviv University, Tel Aviv 69978, Israel

(Received 19 September 1994; accepted 24 January 1995)

Molecular dynamics simulations are used to study solvation and solvation dynamics of a classic charge in a series of ethers of increasing molecular weights, $\text{CH}_3(\text{CH}_2\text{OCH}_2)_n\text{H}$ with $n=1, 2,$ and 4 . Equilibrium structures of the solvated species, ion mobility, linear response solvation functions, and nonequilibrium solvation are studied and compared with the corresponding results for a simple (Stockmayer) fluid. For a typical positive ion, Na^+ , solvation in these systems is found to belong to the nonlinear response regime; the nonlinear behavior is associated with the specific binding of the cation to the negative oxygen sites. Solvation dynamics in the timescale studied ($t < 0.5$ ns) is found to be essentially bimodal, with a short component similar in duration and magnitude to that found in simpler solvents. However, except for the simplest system studied (ethyl methyl ether) the short time component is not Gaussian (i.e., its Gaussian part is limited to insignificantly short times) and cannot be interpreted as inertial free streaming of solvent molecules in the potential field of the solute. Instead we suggest that it originates from damped solvent vibrations about solvent inherent structures. The character of the solvent motions that drive the solvation process changes as the molecular size increases: From overall molecular rotations in the monoether, to intramolecular segmental motions in the larger solvents. It is suggested that solvation dynamics (studied, e.g., by laser induced fluorescence) can be used as a probe for the dynamics of such segmental motions in polymer electrolytes. © 1995 American Institute of Physics.

I. INTRODUCTION

The dynamics of dielectric solvent rearrangement about a newly created charge distribution has been under active study using experimental, theoretical, and numerical techniques.¹ The underlying motivation for these studies is the need to understand the role played by the solvent in the signal observed using ultrafast optical probes of solute molecules and, ultimately, to understand solvent effects on the dynamics of chemical reactions involving solute molecules. In addition, these studies reveal some fundamental issues of dielectric liquid dynamics. In particular, for several protic and aprotic solvents, experimental² and numerical³⁻⁸ studies have shown that the time evolution of solvation is essentially bimodal, with a Gaussian fast response associated with the inertial solvent motions at short times, followed by a slower relaxation that can be accounted for semiquantitatively by continuum dielectric relaxation theory. Numerical simulations with model solvents such as water,³ acetonitrile,⁴ methanol,⁵ methyl chloride,⁶ and a generic Stockmayer model (spherical particles interacting by a combination of Lennard-Jones and point dipole interactions)^{7,8} have indicated that the fast Gaussian response corresponds to more than half the solvation energy. Furthermore, this part of the solvent response has been shown to result from fast cooperative rotation of solvent molecules. Recent theoretical works⁹⁻¹² have also established the importance of this initial underdamped relaxation in simple dielectric solvents. Particularly simple expressions were proposed by Maroncelli *et al.*¹² For ionic solutes in solvents whose relaxation is dominated by point dipole rotations, treated within linear re-

sponse theory and the continuum dielectric approximation, these authors have obtained the following result for the Gaussian relaxation time:

$$\tau_g^{-2} = \frac{1}{2} \alpha_s \langle \omega_1^2 \rangle, \quad (1a)$$

where

$$\langle \omega_1^2 \rangle = k_B T \left(\frac{1}{I_1} + \frac{1}{I_2} + \frac{1}{I_3} \right) \quad (1b)$$

is the thermal square angular velocity of the dipole (k_B is the Boltzmann factor, T is the temperature, and I_i ($i=1,2,3$) are components of the molecular moment of inertia) and α_s is given by

$$\alpha_s = \frac{4 \pi \rho \mu^2}{3 k_B T} \frac{\epsilon_s}{\epsilon_s - 1}, \quad (2)$$

where μ is the solvent molecular dipole moment, ρ —the solvent (number) density, and ϵ_s is the solvent's static dielectric constant. Furthermore, the authors of Ref. 12 have conjectured that the overall LR solvation function $C(t)$ can be approximated by

$$C(t) = [C_1(t)]^{\alpha_s}, \quad (3)$$

where $C_1(t)$ is the single (solvent) molecule reorientational correlation function, i.e.,

$$C_1(t) = \langle \boldsymbol{\mu}(0) \cdot \boldsymbol{\mu}(t) \rangle / \langle \mu^2 \rangle. \quad (4)$$

This conjecture seems to work well in several tested cases, and has been recently shown by Roy and Bagchi^{9(c)} to result, under certain conditions, from a theoretical calculation.

The important role, sometimes dominance, of underdamped relaxation in the solvation dynamics of small solutes in simple solvents raises questions concerning the generality of this behavior and its appearance in more complex systems. While most simulations were done with simple solutes (spherical ions or polar diatomic molecules), recent simulations by Maroncelli *et al.*,¹³ using models of 1-aminonaphthalene and Coumarin 153 in acetonitrile and methanol, have shown that solvation dynamics in these systems is also characterized by a bimodal behavior, however, with a broader initial Gaussian relaxation (i.e., longer Gaussian relaxation time and a smaller Gaussian amplitude) than with the simpler model solutes. This behavior can be traced to the effect of superposition of the responses to the different charge centers in the molecule, as well as to the more hindered motion of the solvent near the more structured solute.

All the theoretical treatments of solvation dynamics cited above have been carried out under the assumption of linear response (LR). The validity of this assumption is far from obvious, since the perturbation associated with changing the charge distribution of typical solutes can be considerable (a change in solvation energy of a few electron volts). Somewhat surprisingly, results based on linear response theory were found to provide good approximations to the actual nonequilibrium behavior of solvation in computer simulations with model solvents such as water,³ acetonitrile,⁴ methyl chloride,⁶ and Stockmayer solvents in a broad range of parameters.^{7,8} This can be checked in several ways. First, the nonequilibrium solvation function

$$S(t) = \frac{E(t) - E(\infty)}{E(0) - E(\infty)}, \quad (5)$$

is equal, in linear response theory, to a corresponding correlation function $C(t)$.¹⁴ For example, for an atomic solute for which the change in charging state marks the onset of the solvation process

$$C(t) \equiv \frac{\langle \delta\Phi(0)\delta\Phi(t) \rangle}{\langle \delta\Phi^2 \rangle}, \quad (6)$$

where Φ is the potential induced by the solvent at the site of the solute. Second, in order that $C(t)$ describes correctly the solvation process it should not depend on the solute's charge between its initial and final values. Finally, LR theory predicts that the denominator (and therefore the numerator) of Eq. (6) should separately be independent of the solute charge. Indeed, $\langle \delta\Phi^2 \rangle$ is directly related (in LR theory) to the solvation energy

$$W_S = -q^2 \langle \delta\Phi^2 \rangle / 2k_B T, \quad (7)$$

where q is the solute's charge. Since $W_S \sim q^2$ in linear response, $\langle \delta\Phi^2 \rangle$ is independent of q . This latter check on the validity of LR is more sensitive than the others, since it avoids cancelations of nonlinear effects by the normalization in Eq. (6). For the Stockmayer solvent model of methyl chloride, with solvent and solute parameters used in Ref. 7, we find that $\langle \delta\Phi^2 \rangle$ changes by $\sim 15\%$ when q changes from 0 to 1 electronic charge (see Fig. 8 below).

Of the model computer solvents studied in recent years, methanol was the only one in which considerable deviations

from linearity were found.⁵ It should be mentioned that (a) the insensitivity of $\langle \delta\Phi^2 \rangle$ to the solute charge was not tried for most of these systems, and (b) recent simulations by Rosenthal *et al.*¹⁵ have shown that methanol stands in less distinction to the other computer solvents studied than originally thought, and that details of the simulated system (e.g., atomic or dipolar solute) strongly influence the character of the response. Thus it appears that relaxation processes dominated by solvent rotations behave more linearly than those dominated by translational motion. This has been recently demonstrated in simulations of solvation dynamics in electrolyte solutions,¹⁶ where a strong dependence of the ionic contribution to the solvation correlation function $C(t)$ on the solute charge was observed. This behavior has been interpreted as resulting from the activated nature of the ion-solvent exchange process at the first solvation layer about the solute, and from the dependence of the corresponding activation barrier on the solute charge. Strong nonlinearity has also been observed in simulations of solvation dynamics in Coulomb lattice gases.¹⁷

As mentioned above, the dependence of the solvation dynamics on the structure of the solute was a subject of several experimental,^{13,18} numerical,¹³ and analytical^{19,20} studies. Less is known about the corresponding effect of solvent structure. An important step in this direction is provided by the theoretical treatments of dielectric response and solvation dynamics in interaction site models of simple solvents by Friedman and co-workers.¹⁰ While these developments go beyond calculations based on point dipole models of the solvents, they are still limited to small rigid systems. Dielectric response theories relate all solvent effects to the dielectric function $\epsilon(\mathbf{k}, \omega)$, however, little is known about this function in solvents of complex nonrigid molecules. Richert and co-workers²¹⁻²³ have made several studies of solvation in glass forming solvents in the supercooled state and near the glass transition temperature. In particular, combined dielectric relaxation and dynamic Stokes-shift measurements were done in 2-methyl tetrahydrofuran with quinoxaline as chromophore, near the glass transition temperature (~ 90 K). Dielectric response is found to obey a Cole- Davidson function, and the corresponding relaxation time—a Vogel-Fulcher-Tammann temperature dependence, as is typical to many glass formers slightly above T_g . Solvation dynamics (represented by the observed Stokes-shift dynamics) is found to be well represented by the dynamic mean spherical approximation.²⁰ However, the time resolution of these experiments is too low to observe possible inertial component(s) in the relaxation.

In a recent study, Chang and Castner²⁴ have compared results of optical-heterodyne-detected Raman induced Kerr effect measurements on three neat liquids; water, ethylene glycol ($C_2H_6O_2$), and triacetin ($C_9H_{14}O_6$); of widely different viscosities. These measurements yield information on the nuclear relaxation dynamics in these liquids, which the authors use, within LR theory and applying Eq. (3), to predict the solvation correlation function. Considerable inertial components in the relaxation are predicted using this procedure, and the prediction made for water is in reasonable agreement with numerical simulations results. The authors note the con-

siderable contribution from inertial response even in solvents with relatively large molecular moment of inertia and slow rotational motion.

It may be concluded from the above discussion that inertial response will dominate solvation dynamics in highly polar small molecule solvents. The relatively slow disappearance of the inertial component as the solvent molecular size increases is associated with the cooperativity effects expressed by the parameter α_s in Eq. (3): When $\alpha_s \gg 1$ the small effect from the initial inertial motion of a single solvent molecule is "amplified." Still, based on this picture we would expect dissipative dynamics to dominate solvation processes in macromolecular hosts where molecular rotation is strongly arrested. However, this expectation disregards relaxation pathways not associated with overall molecular rotations. In fact, the relatively high static dielectric constants observed in macromolecular dielectrics such as polyethers indicates that the dielectric response in such systems is dominated by intrachain or segmental motions which change the local dipole density even as the overall rotation of the chain molecule is frozen. The same types of motion may dominate solvation dynamics in these systems.

In this paper we use molecular dynamics (MD) simulations to study solvation dynamics in a series of model ethers of the form $\text{H}(\text{CH}_2\text{OCH}_2)_n\text{CH}_3$ with $n=1$ (ethyl-methyl ether), $n=2$ (1,2-methoxy ethoxy ethane) and $n=4$. Our focus is on the effect of increasing solvent size and complexity, therefore we limit ourselves to simple "atomic" or "ionic" solutes. Since we expect an increasing importance of intramolecular motions in the solvation process with solvent molecular size we avoid the rigid models used in previous simulations and use fully flexible models for the solvents. Our aim is to compare the dynamics of solvation processes in these solvents and in the simpler solvents studied earlier with respect to (a) the linearity of the response, (b) the existence and amplitude of the "inertial phase" in the response and (c) the relative importance of intramolecular motions.

Our interest in the molecules under study goes further then the issue of solvation dynamics. These molecules are low-molecular weight prototypes of a polyether, polyethylene oxide (PEO). With added salts this host becomes a polymer electrolyte, an ionic conductor above the glass transition temperature.^{25,26} Ionic mobilities in such systems are known to be strongly associated with the local segmental dynamics of the polymer hosts.²⁵⁻²⁷ Solvation dynamics studies in such systems may potentially provide a way to study this motion and its coupling to the ion.

The models studied and details of the simulation are described in the following section. In Sec. III we describe and discuss the results of the simulations. Section IV concludes.

II. MODELS AND METHODS

A. Potentials

The solvents are modeled using the OPLS/Amber force field.²⁸ In this model intermolecular interactions are calculated using OPLS potentials,^{29,30} while intramolecular interactions are derived from the Amber force field.^{31,32} In the OPLS force field the oxygen atoms, the methyls, and the

methylene groups are treated in the united atom representation, i.e., as distinct atomic sites, characterized by partial charges and interacting via Coulombic (C) and Lennard-Jones (LJ) potentials. In the present work the OPLS force field is modified by supplementing all Coulombic interactions by reaction field boundary conditions, whereas electrostatic interactions beyond a cutoff distance R_c are substituted by the response of a dielectric continuum with static dielectric constant ϵ' , taken self-consistently to be approximately equal to that of the solvent. The intermolecular potential between two solvent molecules a and b is thus a combination of C , LJ, and reaction field interactions between atomic sites belonging to the different molecules

$$V_{ab} = \sum_{i(a)} \sum_{j(b)} (V_{ij}^{\text{LJ}} + V_{ij}^{\text{C}}), \quad (8)$$

where $i(a)$ are sites on molecule a and where

$$V_{ij}^{\text{LJ}} = 4\bar{\epsilon}_{ij} \left[\left(\frac{\sigma_{ij}}{r_{ij}} \right)^{12} - \left(\frac{\sigma_{ij}}{r_{ij}} \right)^6 \right] \cdot f_{\text{LJ}}(r_{ij}), \quad (9)$$

$$V_{ij}^{\text{C}} = q_i q_j \left(\frac{1}{r_{ij}} - \frac{\epsilon' - 1}{2\epsilon' + 1} \frac{r_{ij}^2}{R_c^3} \right) \cdot f_{\text{C}}(r_{ij}), \quad (10)$$

and r_{ij} is the distance between sites i and j . In the expression for V_{ij}^{C} the second term in the parentheses arises from the reaction field. $f_{\text{LJ}}(r)$ and $f_{\text{C}}(r)$ are cutoff functions. For f_{LJ} we take a simple step function at $0.8R_c$. For the Coulombic cutoff we use³³

$$f_{\text{C}}(R) = \begin{cases} 1, & R \leq R_s \\ A[R^3 + a_1 R^2 + a_2 R + a_3], & R_s < R < R_c \\ 0, & R_c \leq R \end{cases} \quad (11)$$

where $A = 2(R_c - R_s)^{-3}$, $a_1 = -3/2(R_c + R_s)$, $a_2 = 3R_c R_s$ and $a_3 = -\frac{1}{2}R_c^2(3R_s - R_c)$. With this cutoff function both the truncated Coulombic potential and the force derived from it are continuous at R_s and R_c . In the present calculation we used $R_c = L/2$ and $R_s = 0.95R_c$. Also in the actual calculation Eq. (11) is modified in the following way: Each group of three sites C-O-C defines a neutral dipole (from the parameters listed in Table II $\mu = 1.9161$ D) and a single cutoff function $f_{\text{C}}(R)$, where R is the distance measured from the geometric center of this group, is used for all three sites. However, the actual site-site distances are used for the electrostatic interactions in Eq. (10).

The LJ parameters $\bar{\epsilon}_{ij}$ and σ_{ij} are obtained from the corresponding diagonal interactions using the combination rules $\bar{\epsilon}_{ij} = (\bar{\epsilon}_{ii}\bar{\epsilon}_{jj})^{1/2}$ and $\sigma_{ij} = (\sigma_{ii}\sigma_{jj})^{1/2}$. The values of the partial charges and of the LJ parameters for the intermolecular potentials are listed in Table I.

The intramolecular potential, as adopted from the Amber force field, consists of quadratic terms for the bond stretching and for the nearest neighbor bond angles, cosine terms and scaled 1-4 nonbonded (C and LJ) interactions for the dihedral angle torsions, and full nonbonded interactions between sites further apart along the chain, i.e., by more than three bonds

TABLE I. OPLS parameters (Refs. 30 and 34). The parameters for the ions were obtained from the A^2 and C^2 parameters of OPLS (Ref. 34) by using the relations $A^2=4\bar{\epsilon}\sigma^{12}$ and $C^2=4\bar{\epsilon}\sigma^6$. The parameters taken for the cation are those of Na^+ , except that several values of the charge q were used. For the model anion we took the parameters for Cl^- , except that the value of the LJ parameter σ was taken twice that of Cl^- . R is any aliphatic radical.

Atom or group i	$q_i(e)$	σ_{ii} (Å)	$\bar{\epsilon}_{ii}$ (kcal/mol)	M_i (amu)
O ($R_2\text{O}$)	-0.50	3.0000	0.1700	16
$\text{CH}_2(\text{RCH}_2\text{OR})$	+0.25	3.8000	0.1180	14
$\text{CH}_3(\text{CH}_3\text{OR})$	+0.25	3.8000	0.1700	15
$\text{CH}_3(\text{CH}_3\text{ROR})$	0.00	3.9050	0.1750	15
Model cation	0→2	1.8974	1.6071	23
Model anion	0, -1	8.8344	0.1178	35.5

$$V = \sum_{\text{bonds}} K_r (r - r_{eq})^2 + \sum_{\text{angles}} K_\theta (\theta - \theta_{eq})^2 + \sum_{\text{dih}} \{ (V_0)_{\text{dih}} + V_2(1 + \cos(2\phi)) + V_3(1 + \cos(3\phi)) \} + \sum_i \sum_{j>i+3} \{ V_{ij}^{\text{LJ}} + V_{ij}^{\text{C}} \}. \quad (12)$$

Here, i and j are indices of sites in the molecule, K_r , K_θ , V_2 , and V_3 are constant parameters and $(V_0)_{\text{dih}}$ is given by

$$(V_0)_{\text{dih}} = \frac{1}{8} V_{\text{dih}}^{\text{LJ}} + \frac{1}{2} V_{\text{dih}}^{\text{C}}. \quad (13)$$

V_{ij}^{LJ} and V_{ij}^{C} are given by Eqs. (9) and (10), respectively. The subscript “dih” goes over all pair of sites separated by three bonds and ϕ is the corresponding dihedral angle. The parameters used in the present model are summarized in Table II.

Finally, the additional ion used in the simulation interacts with the solvent molecules by a combination of LJ and Coulombic potentials; the corresponding parameters are listed in Table I. In particular, the cation parameters (except the variable charge) are taken to be the OPLS parameters of

TABLE II. Amber parameters (Refs. 31 and 32).

Bond	r_{eq} (Å)	K_r [kcal/(mol Å ²)]
OCH_2	1.425	320
OCH_3	1.425	320
CH_2CH_2	1.526	260
CH_2CH_3	1.526	260
Angle	θ_{eq} (degrees)	K_θ [kcal/(mol rad ²)]
$\text{CH}_2\text{CH}_2\text{O}$	109.5	80
$\text{CH}_3\text{CH}_2\text{O}$	109.5	80
CH_2OCH_2	111.8	100
CH_3OCH_2	111.8	100
Torsional parameters	V_2 (kcal/mol)	V_3 (kcal/mol)
$\text{OCH}_2\text{CH}_2\text{O}$	0.5	2.000
$\text{CH}_2\text{OCH}_2\text{CH}_3$	0.1	0.725
$\text{CH}_2\text{OCH}_2\text{CH}_2$	0.1	1.450
$\text{CH}_3\text{OCH}_2\text{CH}_3$	0.1	1.450
$\text{CH}_3\text{OCH}_2\text{CH}_2$	0.1	1.450

Na^+ . In the few simulations done with an impurity anion, its radius was arbitrarily chosen as twice the OPLS radius of Cl^- , so as to better represent bigger anions like perchlorate and triflate commonly used in polymer electrolytes.

B. Simulation

Three systems, henceforth denoted I, II, and III were studied. System I contains 100 monoether molecules (400 atoms) in a cubic box of size $L=23.96$ Å. This corresponds to the number density $\rho=7.268 \cdot 10^{-3}$ Å⁻³ which is the experimental value (0.725 g/cm³) for this system at 273 K and 1 atm. System II contains 67 molecules (469 atoms) of the di-ether in a cubic box with $L=23.86$ Å, a density $\rho=4.932 \cdot 10^{-3}$ Å⁻³ (0.853 g/cm³)—the experimental density of 1,2-methoxy ethoxy ethane at room temperature. System III contains 34 molecules (442 atoms) of the tetra-ether in a box of size $L=22.73$ Å, a density $\rho=2.896 \cdot 10^{-3}$ Å⁻³ (0.923 g/cm³) estimated by interpolating between the value of solvent II and the density of $\text{H}(\text{CH}_2\text{OCH}_2)_9\text{H}$ (1.088 g/cm³) estimated for 273 K using $\rho(293 \text{ K})=1.071$ g/cm³ and the thermal expansion coefficient $\alpha=7.8 \cdot 10^{-4}$ °C⁻¹.³⁵ An extra atomic particle (“anion” or “cation”) is added to these systems in order to study the equilibrium response functions and the nonequilibrium relaxation associated with solvation dynamics. The parameters of interaction between this particle and the solvent are given in Table I. Periodic boundary conditions are used with minimal image convention. Again, each C–O–C group is considered as one unit which crosses the boundary when its geometric center does. This is done in order to avoid artifacts resulting from different charged parts of such a group appearing on different sides of the simulation box.

The temperature is kept at 273 K using the Anderson thermalization method.³⁶ The equations of motion are integrated using the velocity Verlet algorithm with a time step $\Delta t=1.097$ fs. Such a small time step is needed since intramolecular dynamics, including stretching vibrations, is not suppressed in this simulation. With this choice of Δt energy is conserved to within 0.1% of its total value over 400 000 steps. In a typical run the system (solvent and solute) is prepared with the molecules at random positions and orientations in the simulation box, with bond lengths and angles initially at equilibrium. An equilibration run of 40 000 time steps was found sufficient in most cases. For high solute charges ($q=1.5$ and 2) 120 000 steps equilibration runs were performed for solvents I and II, while considerably longer runs were needed for solvent III: We have used 380 000 for this purpose. We have also performed a limited set of comparisons with earlier numerical work³⁰ on solvent I. The average site–site pair correlation functions and the relative amount of *gauche/trans* torsional configurations obtained in this solvent are in reasonable agreement with the results obtained using the original OPLS force field in Ref. 30.

Finally, consider the dielectric constant ϵ . It is computed for the pure solvent using³⁷

$$\frac{(\epsilon - 1)(2\epsilon' + 1)}{(2\epsilon' + \epsilon)} = \frac{1}{k_B T R_c^3} (\langle \mathbf{P} \cdot \mathbf{P}(R_c) \rangle - \langle \mathbf{P} \rangle \cdot \langle \mathbf{P}(R_c) \rangle), \quad (14)$$

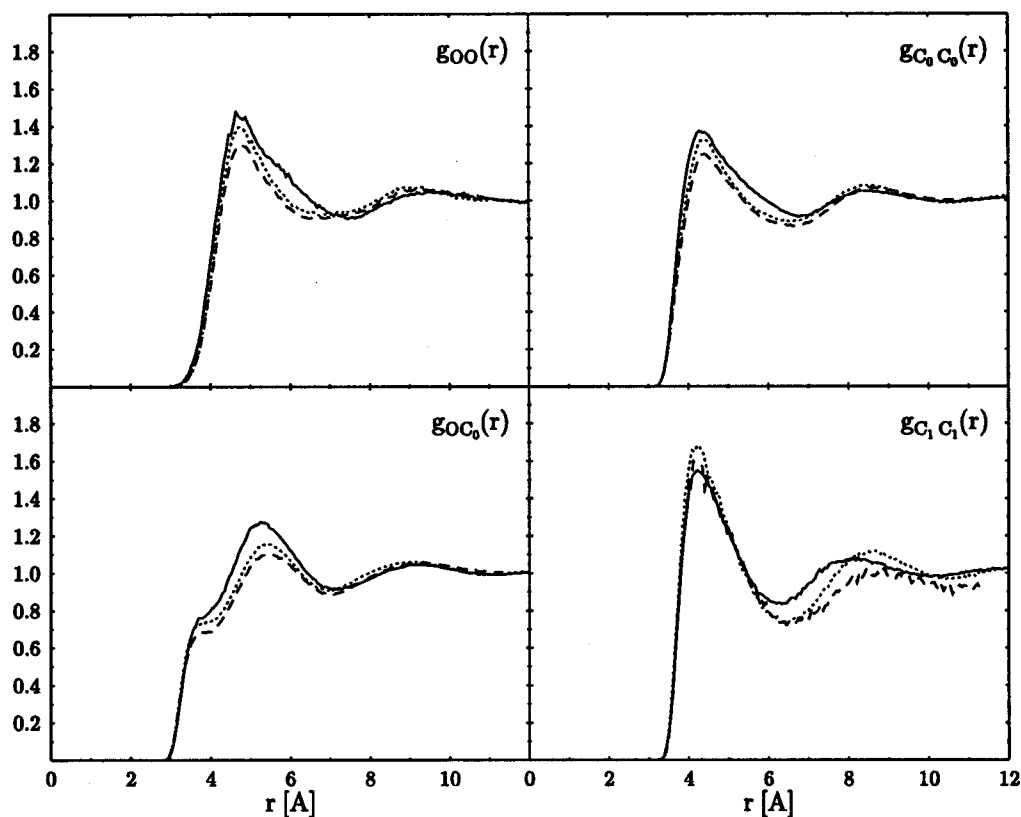


FIG. 1. The intramolecular pair correlation functions $g_{OO}(r)$, $g_{C_0C_0}(r)$, $g_{OC_0}(r)$ and $g_{C_1C_1}(r)$, where C_0 and C_1 are carbon atoms nearest and next nearest to the oxygen atom. Solid line—solvent I. Dotted line—solvent II. Dashed line—solvent III.

where

$$\mathbf{P} = \sum_{i=1}^{N_d} \boldsymbol{\mu}_i \quad (15)$$

and

$$\mathbf{P}(R_c) = \frac{1}{N_d} \sum_{j=1}^{N_d} \left(\sum_{k=1}^{N_d} \boldsymbol{\mu}_k \Theta(R_c - R_{jk}) \right). \quad (16)$$

In Eqs. (15) and (16) $\boldsymbol{\mu}_k$ is the instantaneous dipole moment of the k th dipolar (COC) group, N_d is the number of such groups, R_{jk} is the distance between the geometrical centers of dipolar groups j and k and $\Theta(x)$ is the Heaviside function, $\Theta(x)=1$ for $x \geq 0$ and $\Theta(x)=0$ for $x < 0$. Note that the extra side-methyl group, having no permanent charge, does not affect this calculation. The value of the external dielectric constant ϵ' is determined self-consistently to be the same as that of the simulated system. In the simulations described below ϵ' is taken 10 for system I and 20 for system II. The values calculated from Eq. (14) are 9.8 and 18.2, respectively. For system III we use $\epsilon' = 15$, consistent with the computed dielectric constant, $\epsilon = 16$. We believe, however, that the agreement in solvent III is to some extent accidental: The computed result for this solvent carries a large margin of error resulting from the slow relaxation, hence insufficient sampling, of the equilibrium configurations, in this system.

III. RESULTS AND DISCUSSION

A. Equilibrium simulations: Pure solvents

Figure 1 shows some typical structural pair correlation functions for the pure solvents. It is seen that on this level of description the two ethers are very similar to each other. Figure 2 shows the time correlation function of the center of mass velocity, $C_v(t) = (3k_B T)/(MN) \sum_{i=1}^N \langle \mathbf{v}_i^{(CM)}(0) \mathbf{v}_i^{(CM)}(t) \rangle$ (with N —the number of ether molecules

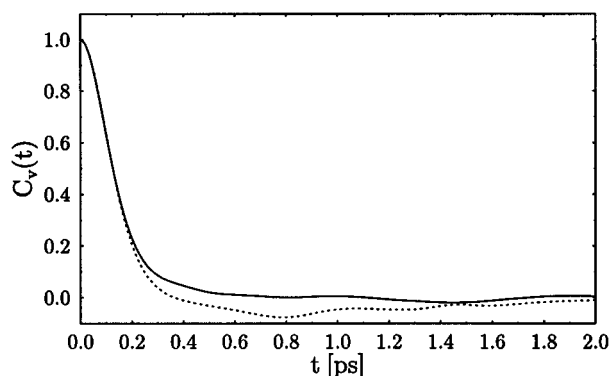


FIG. 2. The center of mass velocity correlation functions $C_v(t)$ for solvents I (full line) and II (dotted line).

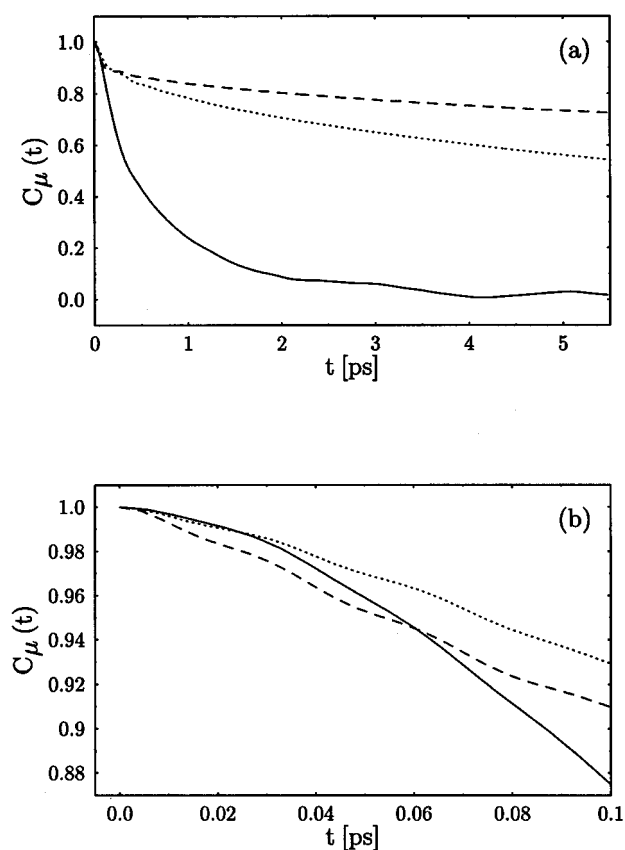


FIG. 3. (a) The dipolar direction correlation functions $C_{\hat{\mu}}(t)$ for solvents I (full line), II (dotted line), and III (dashed line). (b) A closer view of the initial fast decay part of the curves (a).

and M —the molecular mass) for solvents I and II. The tracer diffusion coefficients calculated from these correlation functions are in good agreement with those calculated from the direct computation of mean square distances of migration $\langle(\mathbf{r}^{(\text{CM})}(t) - \mathbf{r}^{(\text{CM})}(0))^2\rangle$: $D^{\text{I}} = 3.9 \cdot 10^{-5}$ cm²/s and $D^{\text{II}} = 1.6 \cdot 10^{-5}$ cm²/s for solvents I and II, respectively.

In Fig. 3(a) the time correlation functions for the molecular dipole direction

$$C_{\hat{\mu}}(t) = \frac{1}{N} \sum_{i=1}^N \langle \hat{\mu}_i(0) \cdot \hat{\mu}_i(t) \rangle \quad (17)$$

with $\hat{\mu} = \boldsymbol{\mu}/\mu$, is displayed. The rotational relaxation becomes successively more hindered as the molecular weight of the solvent increases. The average relaxation times obtained from $\tau_{\hat{\mu}} = \int_0^{\infty} dt C_{\hat{\mu}}(t)$ are $\tau_{\hat{\mu}}^{\text{I}} = 0.774$ ps, $\tau_{\hat{\mu}}^{\text{II}} = 10.3$ ps, and $\tau_{\hat{\mu}}^{\text{III}} = 25.3$ ps. The estimate for solvents II and III were obtained by fitting $C_{\hat{\mu}}(t)$ to a sum of two decaying exponentials, $C_{\hat{\mu}}(t) = B e^{-t/\tau_1} + (1 - B) e^{-t/\tau_2}$ (see below a discussion of this choice) then taking $\tau_{\hat{\mu}} = B \tau_1 + (1 - B) \tau_2$. Note that, since the molecules are nonrigid, the time evolution of $C_{\hat{\mu}}(t)$ does not exactly reflect rotational relaxation.

It is interesting to note that while $C_{\hat{\mu}}(t)$ appears bimodal for the three solvents studied, its short time component is Gaussian-like only for solvent I. This is seen in Fig. 3(b)

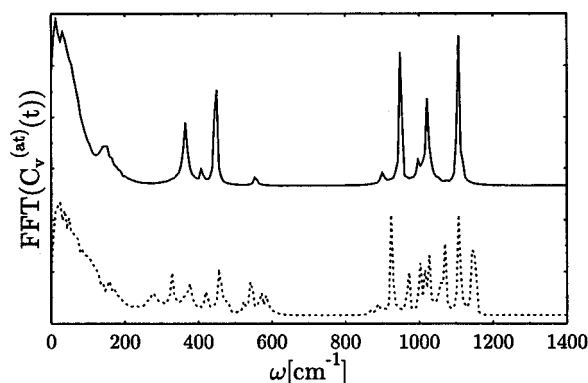


FIG. 4. The spectrum associated with the all-atom velocity correlation function (see the text). Solid line—solvent I, dotted line—solvent II.

which displays the short time ($t \leq 0.1$ ps) relaxation of $C_{\hat{\mu}}(t)$ for solvents I, II, and III. It is seen that an exponential decay, $\exp(-t/\tau_{\text{short}}^e)$, fits better the short time relaxation in the larger solvents, while for solvent I the short time relaxation of $C_{\hat{\mu}}(t)$ is better represented by a Gaussian, $\exp(-(t/\tau_{\text{short}}^g)^2)$. The parameters obtained from these fits are given in Table IV. We note in passing that the short Gaussian relaxation time, $\tau_{\text{short}}^g = 0.27$ ps, obtained for solvent I is in good agreement with that predicted from the Maxwell–Boltzmann distribution of angular velocities according to $(\tau_{\text{short}}^g)^{-2} = (k_B T)/(2)((1/I_1) + (1/I_2) + (1/I_3))$ where I_i ($i=1,2,3$) are the components of the estimated molecular moment of inertia along the molecular principal axes.³⁸

The latter agreement indicates the inertial free streaming nature of the fast relaxation in solvent I. No such correspondence is found for solvents II and III and we may conclude that for these solvents the amplitude of the initial Gaussian evolution is too small to be of any significant physical consequence. We note also that large molecular anisotropies are involved: For example, for solvent I the moment of inertia about the long molecular axis is ~ 13 times smaller than the other two components. Therefore, the averaged thermal frequency $(\tau_{\text{short}}^g)^{-2}$ is dominated by rotation about this axis.

Information pertinent to the short time dynamics of these solvents is also inferred from the spectra obtained from Fourier transforming the corresponding all-atom velocity correlation functions [i.e., the sum over centers of mass in $C_v(t)$ is replaced by a sum over all atomic centers]. These are shown for solvents I and II in Fig. 4. Common to the two solvents is the appearance of three distinct spectral regions centered at ~ 1000 , 400, and below 200 cm⁻¹. By comparing to the spectrum of isolated ether molecules³⁹ the first two regions can be assigned to stretching and bending modes, respectively, while the region below 200 cm⁻¹ contains contributions from the low frequency intramolecular torsions as well as from intermolecular motions. It should be noted that the frequency spectra for the two systems correspond to similar time scales. The different time scales seen in Fig. 3 are associated with differences in the very low frequency end which are not clearly resolved in these spectra.

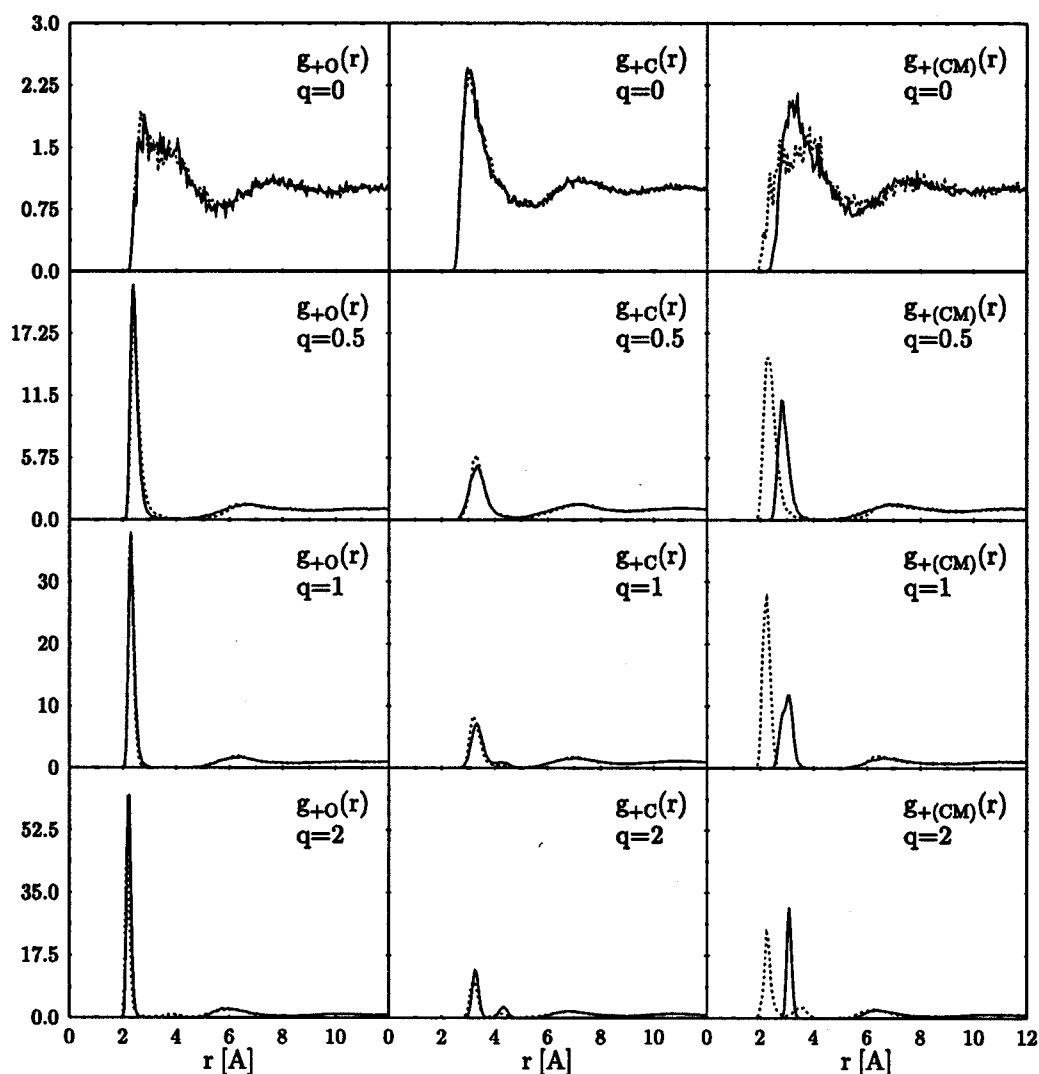


FIG. 5. The correlation functions $g_{+O}(r)$, $g_{+C}(r)$ and $g_{+(CM)}(r)$ for the distributions of oxygen sites, carbon sites, and solvent centers of mass, respectively, about a central ion of charges $q=0$, $q=0.5$, $q=1$, and $q=2$. Full lines: solvent I. Dotted lines: solvent II.

B. Equilibrium simulations of solvation: Energetics and structure

In Fig. 5 we show some pair correlation functions associated with the structure of the solvation shell about a positive ion. The evolution of the solvation structures with increasing solute charge in the range $q=0, \dots, 2e$ is displayed for solvents I and II. Shown are the distribution of oxygen sites, $g_{+O}(r)$, that of carbon sites, $g_{+C}(r)$, and the distribution of solvent molecules centers of mass, $g_{+(CM)}(r)$, about the ion. Note that two somewhat different types of carbon sites contribute to $g_{+C}(r)$. The overall features of these correlation functions are similar in the two solvents. An interesting difference is seen in $g_{+(CM)}(r)$, which for highly positively charged solute shows a first peak in the CM distribution about the ion at a shorter distance from the ion for solvent II than in solvent I. This indicates a tendency for type II molecules to bind to the highly charged cation with both their oxygen sites, thereby bringing the whole solvent

molecule closer to the solute. The position of the first minimum in $g_{+(CM)}(r)$ at ~ 5.25 Å is used below as a measure of the first solvation shell about the ion.

The corresponding results for solvent III are qualitatively similar to those shown for solvents I and II. However, an important technical difference appears: Different trajectories may lead to somewhat different solvation structures which are relatively stable on the time scale of our simulation. This precursor to the phenomenon of inhomogeneous broadening renders our averaging procedure insufficient because within our computing resources we could not sample all possible local structures available to the system.

The equilibrium average of the electrostatic reaction potential induced by the solvent at the solute ion is shown, for solvents I and II as a function of ion charge, in Fig. 6. For comparison we also show here the corresponding results for the Stockmayer fluid of Ref. 7. In linear response theories Φ depends linearly on q , and the free energy of solvation,

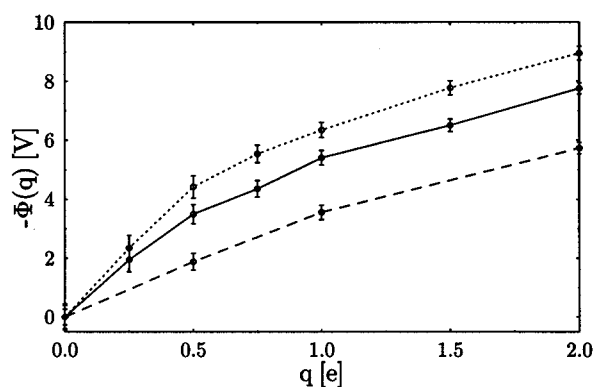


FIG. 6. The equilibrium average of the electrostatic reaction potential Φ induced by the solvent at the solute ion. Full lines: solvent I. Dotted lines: solvent II. Dashed lines: Stockmayer fluid of Ref. 7. The error-bars correspond to $\langle \delta\Phi^2 \rangle^{1/2}$ obtained from the equilibrium simulations.

$\int dq \Phi(q)$, is a quadratic function of q as in the Born theory. Here, deviations from linearity start for both solvents at $q \geq 0.5e$, earlier than in the Stockmayer fluid. The origin of this behavior is seen in Fig. 7, which shows the number of oxygen sites in the first solvation shell surrounding the ion. An approximately linear increase in this number for small q quickly saturates for $q \approx 0.5$. This saturation occurs earlier for solvent II. This can be understood from the fact that the density of oxygen sites in solvent II is 36% larger than in solvent I. Interestingly, our simulations indicate that most of the time these six oxygens come from three solvent molecules. This observation is associated with the fact that the equilibrium torsional angle (the dihedral O-C-C-O angle) in this solvent is approximately 60° , which favors binding of both oxygens to the central cation.

Another manifestation of the nonlinear character of solvation in these systems is seen in Fig. 8, which shows the mean square fluctuation, $\langle \delta\Phi^2 \rangle$, of the solvent induced electrostatic potential at the solute. The linear response expression for this quantity is given by Eq. (7), and is independent of the solute charge q . In contrast, Fig. 8 shows that this quantity depends strongly on q in our systems. Remarkably,

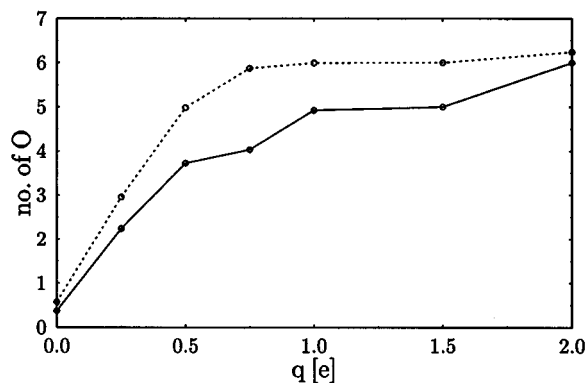


FIG. 7. The number of oxygen sites in the first solvation shell surrounding the ion, within a distance of 2.8 \AA (somewhat beyond the first solvation layer as seen from $g_{+O}(r)$ shown in Fig. 5) of the ion. Full lines: solvent I. Dotted lines: solvent II.

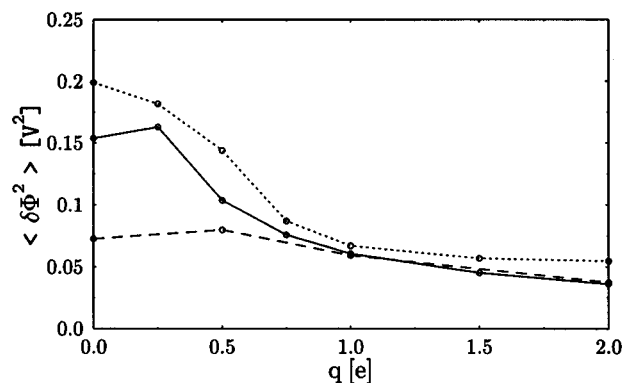


FIG. 8. The mean square fluctuations in the solvent induced electrostatic potential, $\langle \delta\Phi^2 \rangle$, as a function of the solute charge q , for solvent I (full line), solvent II (dotted line), and for the Stockmayer fluid of Ref. 7 (dashed line).

$\langle \delta\Phi^2 \rangle$ is only weakly dependent on q in the Stockmayer solvent, which is a strong indication that the latter system is approximately linear in the corresponding q range. We note in passing that the validity of Eq. (7) is assumed in the derivation of Eq. (1a).

Finally, we have also performed a limited set of simulations for the solvation of the model negative ion (a spherical particle with LJ radius twice that of Cl^-). The results show a much better agreement with linear response predictions, as could have been expected given the much bigger size (i.e., weaker electrostatic interaction) of the anion as well as the fact that the solvation of these species does not involve selective binding to the relatively few oxygen sites.

C. Ion mobility

Table III lists the diffusion coefficients of ions of different charges in solvents I and II. These are obtained from the slopes of the linear $\langle (\delta\mathbf{r})^2 \rangle$ dependence on time. For completeness we have also compared these diffusion coefficients to those of the corresponding pure solvents, and have included also results obtained for the model anion in the same solvents.

TABLE III. Ion diffusion coefficients in systems I and II. $D_{\text{ion}}^{\text{I}}$ and $D_{\text{ion}}^{\text{II}}$ are the coefficients in solvents I and II, respectively. $D^{\text{I}} = 3.9 \times 10^{-5} \text{ cm}^2/\text{s}$ and $D^{\text{II}} = 1.6 \cdot 10^{-5} \text{ cm}^2/\text{s}$ are the corresponding diffusion coefficients of the pure solvents. q is the ion charge (in units of electronic charge). The $q = +0.0$ and $q = -0.0$ species are neutral particles with size equal to that of the cation and anion respectively (see Table I). Due to the large statistical errors (see the text) the numbers in this table should be regarded as rough estimates only.

q	$D_{\text{ion}}^{\text{I}} \times 10^5 \text{ (cm}^2/\text{s)}$	$D_{\text{ion}}^{\text{I}}/D^{\text{I}}$	$D_{\text{ion}}^{\text{II}} \times 10^5 \text{ (cm}^2/\text{s)}$	$D_{\text{ion}}^{\text{II}}/D^{\text{II}}$
0.00	10	2.6	13	8.0
0.25	6.0	1.5	0.9	0.6
0.50	1.7	0.4	0.7	0.4
0.75	1.3	0.3	0.9	0.5
1.00	1.0	0.3	0.6	0.3
1.50	1.1	0.3	0.3	0.2
2.00	0.4	0.1	0.3	0.2
-0.00	2.0	0.5	1.2	0.8
-1.00	2.2	0.6	0.8	0.5

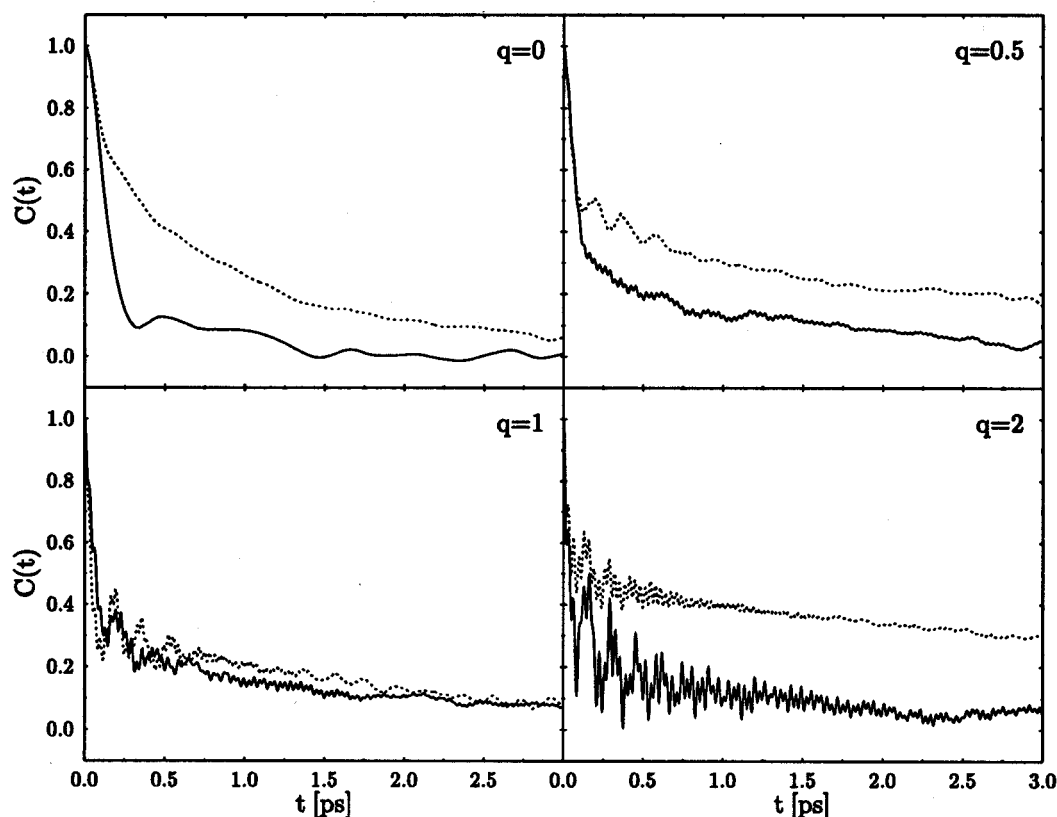


FIG. 9. The linear response solvation functions $C(t)$, Eq. (6), for solvent I (full line) and solvent II (dotted line), for different solute charges: $q=0, 0.5, 1.0$, and 2.0 .

In practice large errors are involved in this estimate because of poor statistics, since only a single ion is considered. The errors in the results given in Table III can be as high as 50%. Nevertheless, several trends are clearly seen: (1) For a neutral solute ($q=0$) the mobility does not depend strongly on the solvent molecular weight, however, this changes drastically when the solute becomes charged. (2) The drop in the ion mobility upon increasing charge is very sudden in solvent II and relatively more gradual in solvent I. In neither it behaves according to expectations based on LR theory, $D \sim (C_1 + C_2 q^2)^{-1}$.⁴⁰ Both observations can be rationalized by the strong binding between the positive ion and the negative oxygen sites. Because of this binding the relatively weak dependence of the neutral species mobility on the solvent becomes strongly host controlled upon charging; the effect being more pronounced in solvent II, as could have been expected from the behavior displayed in Fig. 7.

Larger, more weakly bound anions such as perchlorate or triflate are known to be more mobile than the small Li^+ or Na^+ cations.²⁵ This is also observed in our simulations as seen in Table III. For neutral solutes, because of the much larger size, the large “anionic” species diffuse considerably more slowly than the cationic species. This is reversed in the charged solutes where the stronger binding of the cation to the solvent renders it less mobile.

D. Solvation dynamics

Consider first the linear response solvation function $C(t)$, Eq. (6). Figure 9 shows these functions for solvents I and II for different solute charges, obtained from long (~ 400 ps) equilibrium trajectories. As in simpler solvents studied earlier, these functions show an essentially bimodal relaxation with superimposed oscillations. We first disregard these oscillations and focus on the two main relaxation components. The slow component which dominates the long time part of the relaxation can be fitted to an exponential function

$$C(t) \sim A e^{-t/\tau_{\text{long}}} \quad (18)$$

with the characteristic time τ_{long} . The fast component corresponds to that observed in simple solvents, that was shown to be Gaussian-like and interpreted as arising from “inertial” free streaming of solvent molecules on a time scale shorter than intermolecular collisions, as discussed in Sec. I. The present situation is less obvious, and a closer look at the short time relaxation reveals a different picture that could have been anticipated from Fig. 3(b). In Figs. 10 and 11 we show the short time, $t \leq 0.1$ ps, part of the evolution seen in Fig. 9. For a neutral solute in solvent I a Gaussian fit works well, but as the solute charge increases an exponential relaxation (linear decrease on this time scale) seems to fit the observed evolution better if oscillations associated with local

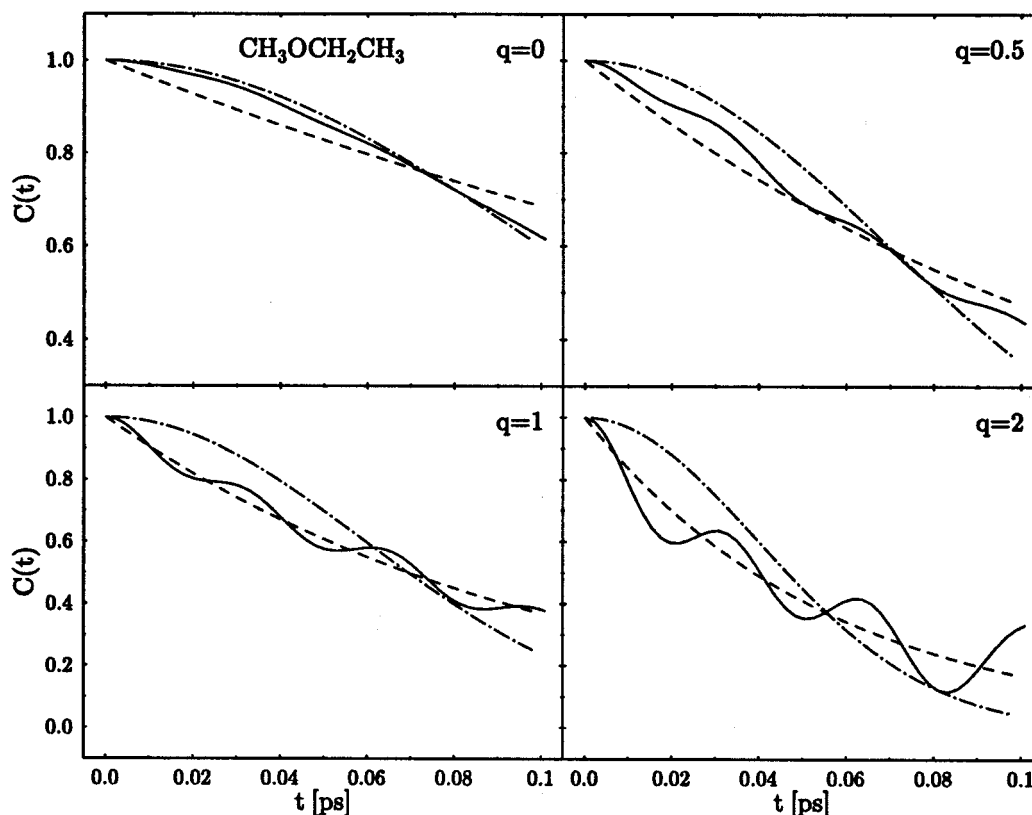


FIG. 10. Solid lines: Expanded short time segments from Fig. 9 of the correlation function $C(t)$ for solvent I. Dashed lines: Best fits to an exponential function, $e^{-t/\tau_{\text{short}}^e}$. Dashed-dotted lines: Best fits to a Gaussian, $e^{-(t/\tau_{\text{short}}^g)^2}$. The parameters obtained from these fits are listed in Table IV.

libration and solvent internal vibrations are disregarded. For solvent II the short time component is represented better by an exponential relaxation for all solute charges, including $q=0$. We arrive at the surprising conclusion that even though the time evolution of the linear response solvation function $C(t)$ is essentially bimodal, the fast component cannot be interpreted as inertial free streaming motion of solvent molecules, except for the simplest solute/solvent system studied. It should be emphasized that an initial Gaussian evolution is implied by fundamental theoretical considerations. It appears tough that for solvent II and for solvent I with a highly charged solute this Gaussian evolution is limited to physically insignificant short times and that, nevertheless, the evolution on the picosecond time scale is bimodal. We conclude that depending on the system studied, the short time component can have a Gaussian or an exponential character

$$C(t) = e^{-(t/\tau_{\text{short}}^g)^2} \quad \text{or} \quad C(t) = e^{-t/\tau_{\text{short}}^e}, \quad (19)$$

with the exponential becoming the better representation for the larger solvents. In Table IV the parameters obtained from such fits for solvents I and II are listed.

It is common to fit such bimodal relaxations to a linear combination of simple decay functions. In the present case obvious choices are

$$C(t) = A e^{-(t/\tau_g)^2} + (1-A) e^{-t/\tau_e}, \quad (20)$$

$$C(t) = B e^{-t/\tau_1} + (1-B) e^{-t/\tau_2}. \quad (21)$$

We note that these forms have no physical basis and are in fact wrong at $t \rightarrow 0$. However, they can provide useful expressions in practical applications. Based on the above discussion, we expect form (20) to fail in many of the systems studied here, in contrast to what was found in simpler solvents. As an example, Fig. 12 shows the function $S(t)$ for the process $q=0 \rightarrow q=1$ for solvent II (also shown in Fig. 20) with the corresponding fits to Eqs. (20) and (21). Obviously Eq. (21) provides a much better fit.

A note of caution should be made on the quality of the results displayed in Figs. 9–11 and in Table IV. Since only a single solute particle is involved, the result may depend on the environment of the particle. This should not constitute a problem for $q \leq 1$, however, for larger charges the local solvent structure about the solute may be arrested in a particular configuration (e.g., a given number of solvent molecules contributing the oxygens in the first solvation shell) and a good sampling of all possible configurations may not be achieved even with the long trajectory (440 ps) used. This results in a larger margin of error.

To summarize, the following observations can be made on the results for the linear response function $C(t)$: (a) Excluding high frequency oscillations associated with solvent librations in the field of the solute and with solvent intramolecular motion, the time dependence of $C(t)$ is essentially bimodal, displaying a fast and a slow component on the time scale studied. The existence of slower relaxation components

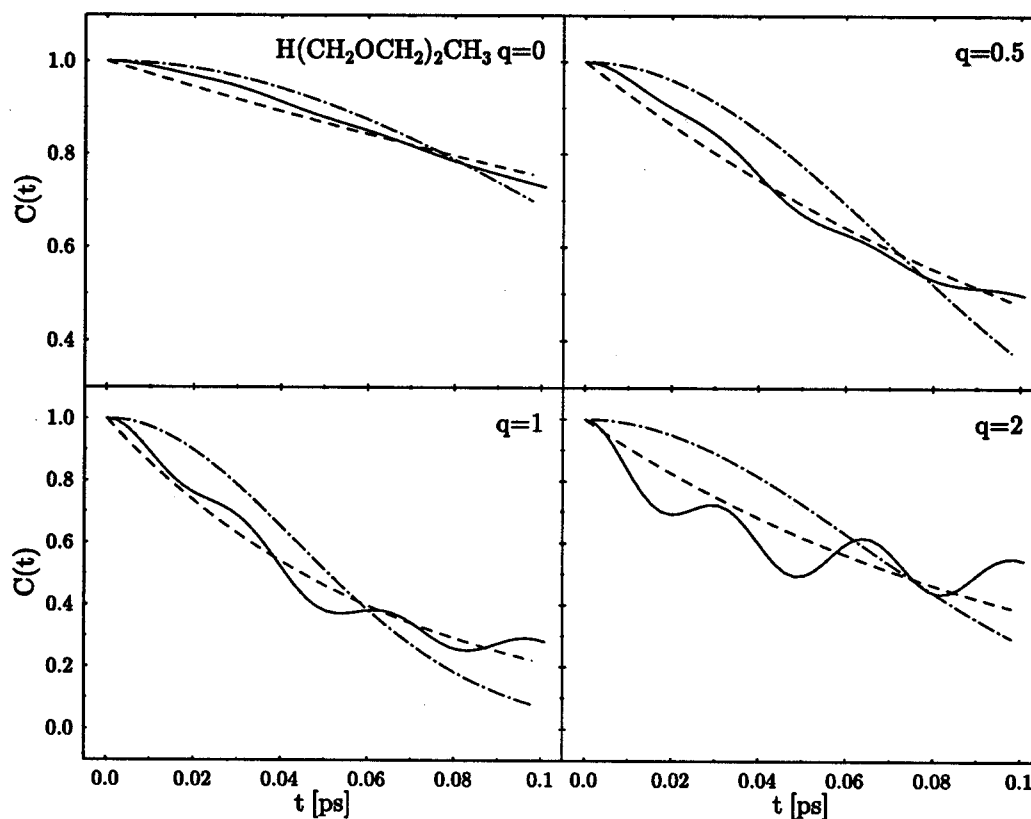


FIG. 11. Same as Fig. 10, for solvent II.

cannot, indeed should not,^{21–23} be ruled out. (b) $C(t)$ depends strongly on the solute charge. In particular, the initial relaxation becomes faster as q increases. The other, slow component, depends strongly on the solvent and is considerably slower for the more complex solvent II. (It is even slower in solvent III, see below). (c) The fast component accounts for at least half of the relaxation in all cases studied, except for the neutral ion in solvent II (and III, see below). (d) As discussed above the fast component does not in gen-

eral correspond to the inertial free streaming motion which appears to dominate this component in simpler solvents.

It is of interest to compare these numerical results to the linear response—continuum dielectric results (1)–(2) as well as the conjecture (3). The relevant results are those associated with a neutral solute, $q=0$. α_s , Eq. (2), is calculated using parameters obtained from the simulations; the needed

TABLE IV. Parameters obtained from fitting the time evolution of the equilibrium correlation functions $C(t)$ [Eq. (6)], $C_{\hat{\mu}}(t)$ [Eq. (17)], and $C_1(t)$ [Eq. (4)] and the nonequilibrium solvation function $S(t)$ [Eq. (5)] to analytical functions. The parameters A and τ_{long} were obtained from fitting the results for $0.5 \text{ ps} < t < 3.0 \text{ ps}$ to the exponential form $Ae^{-t/\tau_{\text{long}}}$. The parameters τ_{short}^e and τ_{short}^g were obtained by fitting the computed results for $t < 0.1 \text{ ps}$ to the forms $e^{-t/\tau_{\text{short}}^e}$ and $e^{-(t/\tau_{\text{short}}^g)^2}$, respectively.

	$q(e)$	A^I	τ_{long}^I (ps)	$\tau_{\text{short}}^{g,I}$ (ps)	$\tau_{\text{short}}^{e,I}$ (ps)	A^{II}	τ_{long}^{II} (ps)	$\tau_{\text{short}}^{g,II}$ (ps)	$\tau_{\text{short}}^{e,II}$ (ps)
$C(t)$	0.00	0.351	0.555	0.140	0.265	0.600	1.209	0.164	0.350
	0.25	0.392	0.781	0.120	0.197	0.470	2.714	0.121	0.197
	0.50	0.260	1.703	0.0978	0.134	0.413	3.351	0.0991	0.136
	0.75	0.304	1.858	0.0963	0.128	0.324	2.196	0.0687	0.0758
	1.00	0.252	2.226	0.0834	0.100	0.337	2.052	0.0614	0.0650
	1.50	0.306	1.279	0.0741	0.0820	0.330	3.493	0.0751	0.0825
$S(t)$	0→0.25	0.197	1.898	0.0561	0.0562	0.464	6.325	0.0886	0.105
	0→0.50	0.566	0.696	0.149	0.297	0.551	1.795	0.169	0.372
	0→1.00	0.450	1.115	0.147	0.287	0.502	2.475	0.166	0.359
	1→0.00	0.369	1.799	0.138	0.253	0.410	2.116	0.145	0.273
$C_{\hat{\mu}}(t)$		0.0326	4.266	0.117	0.186	0.242	1.538	0.0925	0.122
$C_1(t)$		0.670	0.999	0.265	0.918	0.867	10.00	0.342	1.468
		0.669	0.999	0.262	0.894	0.875	10.71	0.359	1.610

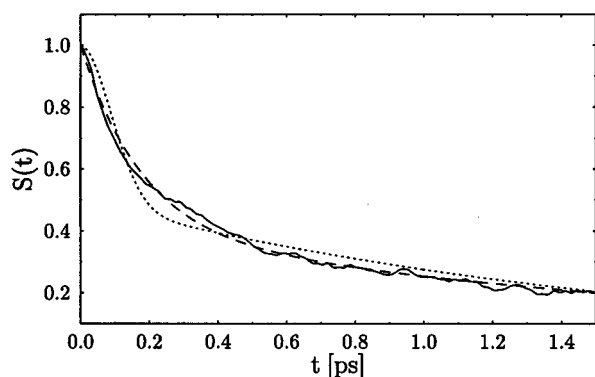


FIG. 12. Solvation function $S_{0 \rightarrow 1}(t)$ (solid line) for solvent II and its best fits to Eq. (20) (dotted line) and Eq. (21) (dashed line). These fits were obtained in the interval $0 \leq t \leq 3.0$ ps. Only part of the interval is shown.

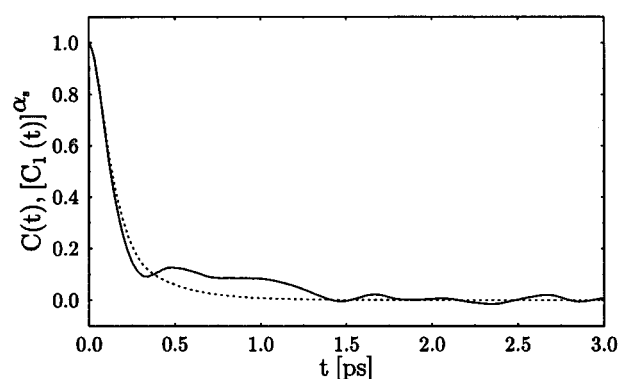


FIG. 13. A comparison between $C(t)$, Eq. (6), (solid line) and $[C_1(t)]^{\alpha_s}$, Eqs. (3) and (4), (dotted line) for solvent I.

data is summarized in Table V. Anticipating later discussion below we have used two extreme models for the solvents II and III. In one, ρ is the molecular density and μ is the total molecular dipole averaged over all solvent molecules along the trajectory. In the other we have used $\rho^{(i)}$ and $\mu^{(i)}$ —the density and dipole moments of individual C–O–C groups, as if these groups behave as individual molecules. It is seen that the values of $\alpha_s^{(i)}$ and α_s differ from each other by no more than 20%.

The results of these calculations can be summarized as follows:

(1) Eq. (1a) is satisfied to a reasonable level of accuracy for solvent I: $(\tau_{\text{short}}^g)^{-2}$ is 51.0 ps^{-2} for $C(t)$ (with $q=0$) and 14.6 ps^{-2} for $C_1(t)$ Eq. (4) [practically identical to $C_{\hat{\mu}}(t)$, Eq. (17), for this solvent] while $\alpha_s = \alpha_s^{(i)} = 3.33$ (from Table V). For solvents II and III we find that an equivalent relation $\tau_{\text{short}, \Phi}^e = \alpha_s^{-1} \tau_{\text{short}, \mu}^e$ between the exponential relaxation times of the short components of $C(t)$ and $C_1(t)$ is satisfied approximately.

(2) While the success of Eq. (1) for solvent I can be rationalized along the lines discussed in Ref. 12 the success of the equivalent relation for solvents II and III can only be associated at present with the conjecture (3). Indeed, conjecture (3) appears to be satisfied reasonably well for all systems studied. This is seen in Figs. 13–15 which compare the time evolution of $C(t)$ and $[C_1(t)]^{\alpha_s}$ for solvents I–III. For solvents II and III we have used two different procedures to calculate $[C_1(t)]^{\alpha_s}$: one based on the overall molecular dipoles in the calculation of $C_1(t)$ [Eq. (4)] and α_s , and the other based on the individual C–O–C dipoles as the dynamical variables in Eq. (4), together with replacing α_s by $\alpha_s^{(i)}$ in the conjecture (3). The results as seen in Figs. 14 and 15 are

quite similar, especially at short times. The implications of these observations deserve further theoretical and numerical study.

The most striking observation in the results presented above is the similarity between the time scales of solvation seen in two solvents whose characteristic time scales for rotational diffusion are vastly different. As discussed in Sec. I, this points out to the importance of intramolecular, segmental motion in the dynamics of solvation in chain-molecule solvents. Obviously, the two solvents that were studied in detail are not good examples of chain molecules. We have also carried out a limited set of linear response studies with solvent III. As seen in Fig. 3, overall molecular rotation is practically absent in this solvent on our time scale. However, solvation dynamics, as expressed by the LR function $C(t)$ proceeds as efficiently as in solvent II. Figure 16 compares the computed functions $C(t)$ for the three solvents under study. The short relaxation times obtained from fitting to the exponential $e^{-t/\tau_{\text{short}}^e}$ are 0.365 and 0.106 ps for solvent III with $q=0$ and $q=1$, respectively, quite similar to that of solvents I and II (see Table IV). The main difference observed is the considerably larger amplitude of the short relaxation component in solvent I with $q=0$. Remarkably, no such difference is seen for $q=1$, where the relaxation is very similar in the three solvents, except that the long time relaxation is somewhat slower in the tetra-ether. This similarity is striking also in view of the fact that the density in solvent III is $\sim 30\%$ larger than that of solvent I. Also striking is the semiquantitative agreement between $C^{\text{III}}(t)$ and $[C_1^{\text{III}}(t)]^{\alpha_s}$ ($\alpha_s = 5.86$) as seen in Fig. 15.

The oscillations superimposed on the otherwise bimodal relaxation of $C(t)$ are associated with librations of solvent

TABLE V. Physical properties of solvents I–III used to calculate α_s from Eq. (2). The quantities marked with superscript i correspond to the individual C–O–C dipoles as the basic entities in the calculations.

Solvent	ϵ_s	$\mu^{(i)}$ (D)	$\rho^{(i)} \times 10^3$ (\AA^{-3})	$\alpha_s^{(i)}$	μ (D)	$\rho \times 10^3$ (\AA^{-3})	α_s
I	10				1.927	7.268	3.33
II	20	1.927	9.865	4.288	3.040	4.932	5.34
III	15	1.927	11.584	5.087	4.131	2.896	5.86

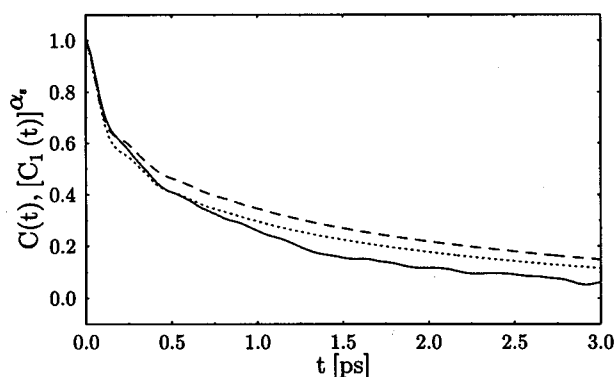


FIG. 14. Same as Fig. 13 for solvent II. Additionally, the dashed line represents $[C_1(t)]^{\alpha_s^{(i)}}$, where $C_1(t)$ and $\alpha_s^{(i)}$ are calculated for the individual C–O–C dipoles (see the text).

molecules in the field of the solute and with intramolecular solvent motion. The corresponding spectrum is obtained by taking the Fourier transform ($t \rightarrow \omega$) of $C(t)$. Examples of the resulting spectrum are seen in Figs. 17 and 18. As q increases the contribution from both intramolecular and intermolecular solvent modes become more pronounced and a low frequency band near 200 cm^{-1} is strongly pushed to higher frequencies. The latter observation indicates that this peak is probably associated with cage modes—translations of the ion in its solvation cage and/or libration of nearest neighbor solvent dipoles in the solute's field.

The strong dependence of $C(t)$ on the solute charge implies that this linear response function does not provide a good description of the actual nonequilibrium solvation process. This is indeed seen in Figs. 19 and 20 where the non-equilibrium solvation functions [Eq. (5)] $S_{0 \rightarrow 1}(t)$ and $S_{1 \rightarrow 0}(t)$ calculated following jumps in the solute charge from 0 to 1 and from 1 to 0, respectively, are shown for solvents I and II together with the linear response functions $C(t)$ (already shown in Fig. 9) obtained from equilibrium trajectories with solutes of charge 0 and 1. The parameters obtained from fitting these functions to the forms (18) and (19) are given in Table IV. The qualitative behavior of $C(t)$ and $S(t)$ is seen to be very similar. In particular, a prominent fast component whose magnitude is similar in solvents I and

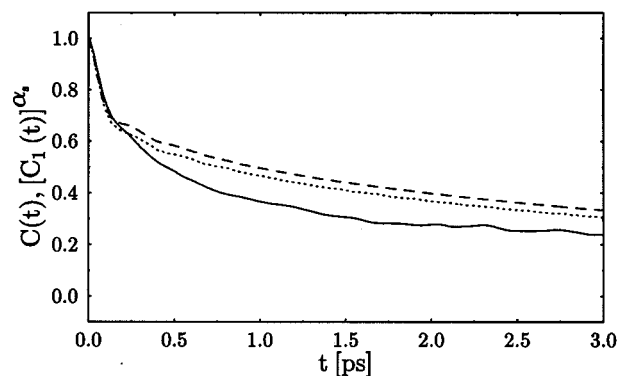


FIG. 15. Same as Figs. 13 and 14 for solvent III.

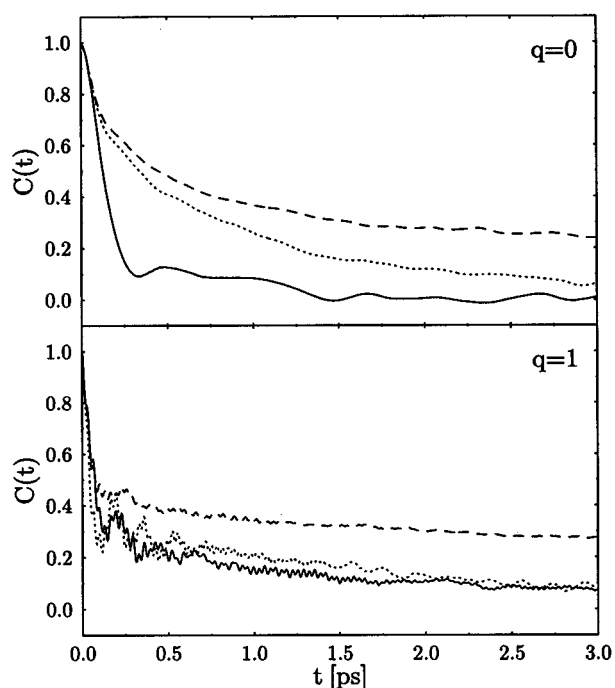


FIG. 16. The correlation function $C(t)$ for the solvent I (full line), solvent II (dotted line), and solvent III (dashed line), for neutral ($q=0$) and charged ($q=1$) solutes.

II exists in both cases. There are, however, large quantitative differences between the different solvation functions.

It is interesting to look at the time evolution of some other structural and energetic quantities during the nonequilibrium solvation process. A qualitative difference between solvent I and the larger polyethers is that the dipole vector in solvent I can change considerably only by molecular rotation while for larger solvents this may result also from intramolecular distortion. To demonstrate these different effects we show in Figs. 21–23 the time evolution of several structural

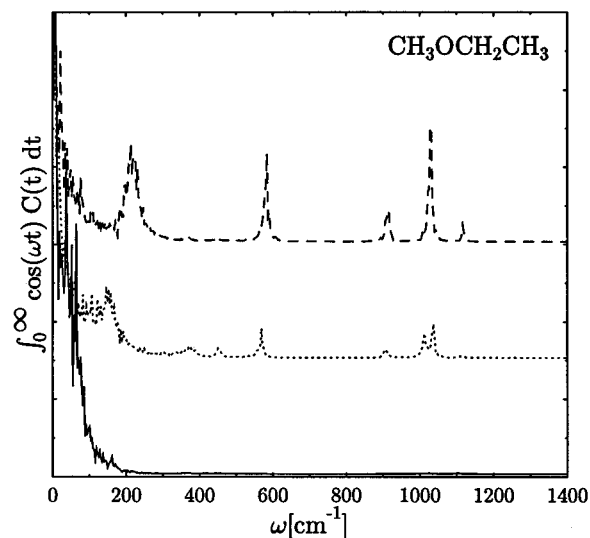


FIG. 17. A spectral representation of the linear response solvation function $C(t)$ for solvent I. Full line: $q=0$, dotted line: $q=1$, dashed line: $q=2$.

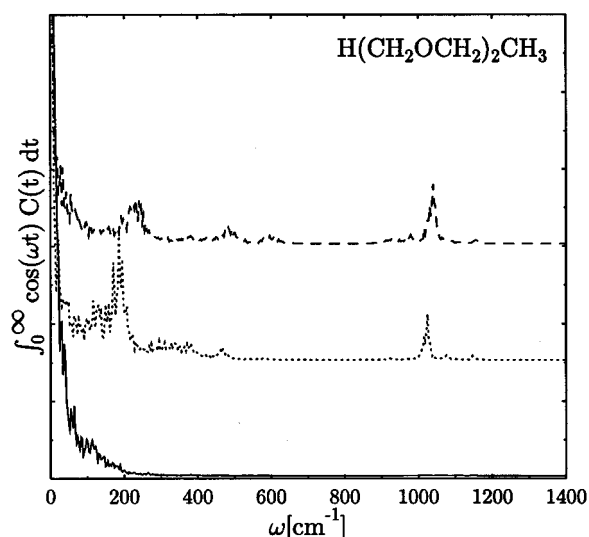


FIG. 18. Same as Fig 17 for solvent II.

properties of solvent molecules in the first solvation layer about the solute (within 5.25 Å from the ion center), in solvents I and II, following a jump in the solute charge from $q=0$ to $q=1$. Figure 21 shows the time evolution of the angle ϕ between the direction of the solvent molecular dipole and the line connecting the solute center with the center of mass of the solvent molecule. For comparison the number of oxygen sites in the first solvation shell is also shown. Obviously, the initial response is dominated by rotational motions rather than by exchanging solvent carbons near the solute by solvent oxygens. Figure 22 compares the evolutions of the magnitudes μ of the averaged molecular dipole (in the first solvation shell) in solvents I and II. As expected no systematic evolution is seen in solvent I while a considerable change is seen in solvent II. The origin of this change is seen in Fig. 23, which shows the time evolution of the angle ϕ_{12} between the dipoles of the individual C–O–C groups in solvent II, averaged over 40 trajectories following the jump in the solute charge. During the first 0.2 ps this angle changes from $\sim 81^\circ$ to $\sim 66^\circ$. The overall time evolution seen in Figs. 22 and 23 is also remarkable: Following a

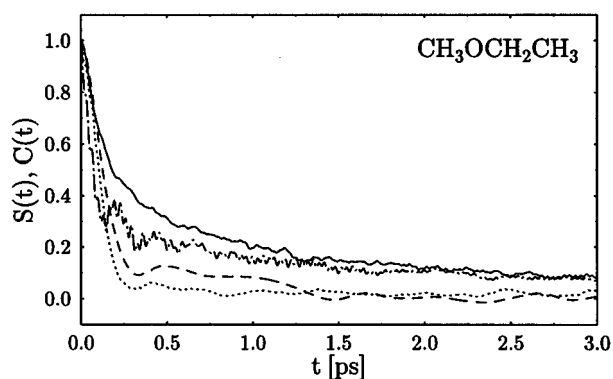
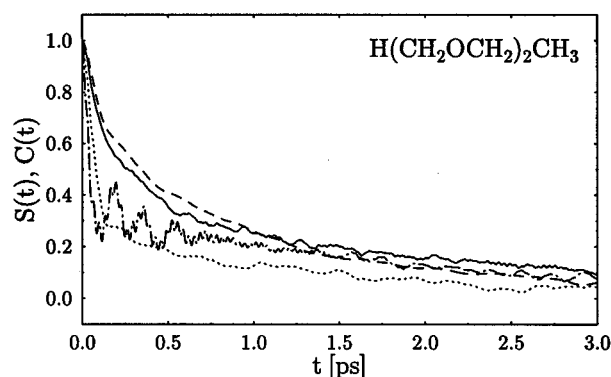
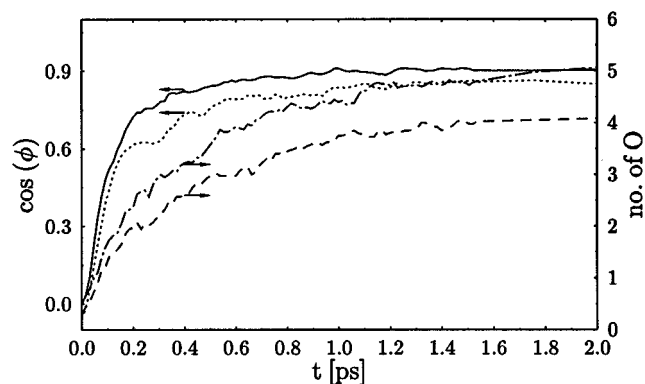
FIG. 19. Solvation and response functions for solvent I. Full line: $S_{0 \rightarrow 1}(t)$; dotted line: $S_{1 \rightarrow 0}(t)$. Dashed line: $C(t)|_{q=0}$; dashed-dotted line $C(t)|_{q=1}$.

FIG. 20. Same as Fig. 19, for solvent II.

rapid change in the internal angle from $\sim 81^\circ$ to 66° , a subsequent slow relaxation takes place which bring this angle to the final equilibrium value $\sim 71^\circ$ [which characterize solvent II molecules in the first solvation layer about a positively charged ($q=1$) ion].

Another quantity of interest is the solvent temperature in the vicinity of the solute, following the solute charge jump. The relaxation of this variable may have implications on the time dependent optical response of the solute following the sudden jump in its charge distribution. Focusing again on solvent molecules whose center of mass is located within 5.25 Å from the ion (roughly the first solvation shell), the time evolution of the associated local temperature following a $q=0 \rightarrow q=1$ jump is displayed in Fig. 24. Here, the behavior of the two solvents is very similar; the slightly lower temperature attained in the case of solvent II can be attributed to the higher density of this solvents. The temperature rises, essentially on the time scale of the initial Gaussian, to about two times its equilibrium temperature of 273 K, then relaxes approximately exponentially.

FIG. 21. The time evolution of $\cos \phi$, where ϕ is the angle between the line connecting the ion to the center of mass of solvent molecules in the first solvation shell and between the dipole of the same molecule, averaged over these molecules. A jump $q=0 \rightarrow q=1$ in the solute charge takes place at $t=0$. Full line: solvent I. Dotted line: solvent II. For comparison, the time evolutions of the number of oxygen sites near the solute (at distances smaller than 2.8 Å) is shown. Dashed line: solvent I. Dashed-dotted line: solvent II.

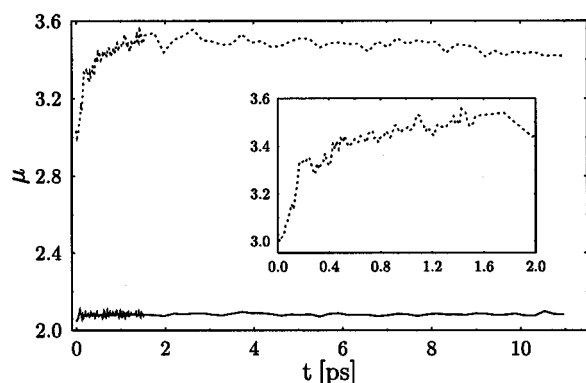


FIG. 22. The time evolution of the magnitude μ of the molecular dipole of solvent molecules in the first solvation layer about the solute (averaged over solvent molecules in that layer) following a jump $q=0 \rightarrow q=1$ in the solute charge. Full line: solvent I. Dotted line: solvent II. The insert show the time segment of the same data for solvent II.

Earlier simulations of solvation dynamics in simple solvents have characterized the initial fast component of the time evolution as free streaming motion of solvent molecules in the newly modified electric field of the solute. The results of the present study show that as the solvent becomes more complex, and its motion more strongly hindered, the free streaming part of its response is physically insignificant. Nevertheless, the relaxation is still largely bimodal (more than two time scales are observed even on our time window as seen, e.g., in Figs. 22 and 23) with the fast component relaxing on a time scale similar to that in the simplest solvent in the series studied. It appears that the bimodal nature of the solvation originates from a yet undetermined source not directly related to the initial Gaussian relaxation associated with the free streaming motion. *Whatever the origin of this fast component is, it is only in simple solvents, with relatively unhindered molecular rotations, that this component can be viewed as independent motions of noninteracting modes.* In solvents II and III the fast component exists but its dynamics is strongly affected by solvent–solvent interactions, and considerable deviations from Gaussian evolution appear.

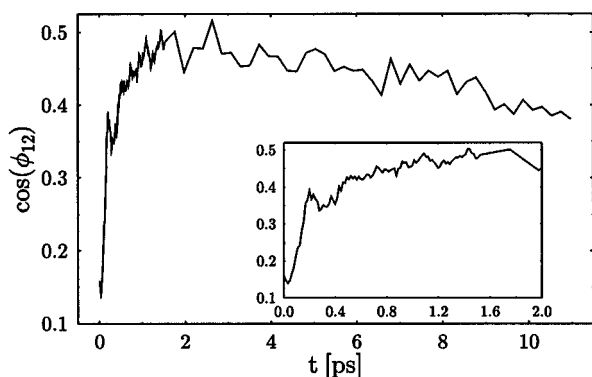


FIG. 23. The time evolution of the internal angle ϕ_{12} between the directions of the individual C–O–C dipoles in solvent II following a $q=0 \rightarrow q=1$ jump at $t=0$. The insert show the short time segment of the same data.

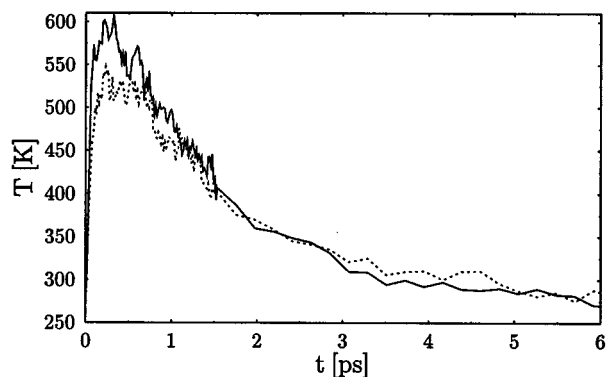


FIG. 24. Temperature of the first solvation shell following a $q=0 \rightarrow q=1$ jump in the solute charge. Full line: solvent I, dotted: solvent II.

Since the pronounced bimodal evolution characterizes not only the nonequilibrium solvation function $S(t)$ but also the equilibrium correlation functions $C(t)$ and $C_{\dot{\mu}}(t)$, it is enough to consider the latter. A conjecture about the origin of the bimodal behavior may be made as follows: The motion in configuration space of a liquid is a combination of fluctuations about minima associated with inherent structures (only this motion remains when the liquid freezes and becomes an amorphous solid) and larger amplitude activated transitions between wells associated with different inherent structures. It seems reasonable to associate the fast component of the response with the former motions which do not involve activated barrier crossings along some “reaction coordinate” and the slower component(s) with the large amplitude transitions between inherent structures. It should be remembered that the relevant solvent motions are those that strongly affect the potential at the solute. These are coupled to the rest of the solvent degrees of freedom and it is the effectiveness of this coupling on the time scale of the short component and the associated dissipation of the local motions that will determine whether the short time relaxation is dominated by the free streaming or dissipative dynamics. Further discussion of these issues will be presented elsewhere.

IV. CONCLUSIONS

We have studied solvation dynamics in a series of solvents with increasing complexity and have found significant differences in the response of such solvents to a sudden change in the solute’s charge distribution relative to earlier results obtained for simple solvents. First, linear response theory does not provide a good representation of the solvation in the polyether solvents studied. We have argued that this nonlinear behavior is associated with the carbon–oxygen exchange process in the vicinity of the driving ion. Second, as the solvent molecular size increases the short time solvation dynamics is dominated by intramolecular segmental motions as opposed by overall molecular rotation. The time scale for this process is similar to that observed in simpler solvents which is controlled by rotational motion of the solvent molecules. The success of relation (3) in predicting the short time dynamics deserves further studies. Finally, solvation dynamics is bimodal and the gross features of the cor-

responding time evolution are similar to those observed in simpler solvents. For the larger solvents used in the present study the short time component is, however, not Gaussian (except of a negligibly short time segment) and is better fitted by an exponential relaxation. We have suggested this bimodal nature of the relaxation process is associated with solvent libration about inherent solvent structures followed by relatively rare events of activated solvent structural changes. This picture of solvent dynamics has been under discussion for some time.⁴¹

Spectroscopic studies of solvent response to changes in the solute's charge distribution provide a direct probe of the solvent dynamics about a solvated ion both on the time scales studied in the present work and on the much longer time scales studied in Refs. 21–23. This may prove useful particularly in the context of polymer ionic conductors because segmental motions of the polymer chains which are instrumental in controlling ion mobility also appear to drive the solvation process. Similar techniques can be used to monitor ionic motion in solid ionic conductors, as recently demonstrated by Huppert and co-workers.⁴²

Solvent dynamics can play a major role in the mechanism and rate of chemical reactions involving dissolved species. In particular, solvent dynamical effects on the rate of electron transfer have been under intense study. There is some evidence^{43,44} that electron transfer reactions are slower in polymer hosts than in simple dielectric solvents, but it is not clear from the available data if this is related to the slower diffusion in the polymer or to direct solvent dynamical effect on the electron transfer process. Our simulations show that the electrostatic potential fluctuations about a central ion are similar in magnitude and time scale in most systems studied. This would suggest that the reported observations are associated with the slower diffusion process, however, this cannot be stated conclusively since the longer time scales that appear in the potential fluctuations do slow down when the host molecular weight increases. Intramolecular electron transfer processes, which do not involve reactant diffusion, may provide the needed experimental information concerning this point.

ACKNOWLEDGMENTS

This work was supported by the Israel Science Foundation, by the U.S.–Israel Binational Science Foundation and by the Kurt Leon Foundation. We thank Professor W. Dieterich, Professor D. Huppert, Professor M. Maroncelli, and Professor M. Ratner and Dr. E. Neria for helpful discussions and for works sent to us prior to publication.

¹(a) For a review see M. Maroncelli, *J. Mol. Liq.* **57**, 1 (1993); (b) *AIP Conf. Proc.* **298**: "Ultrafast Reaction Dynamics and Solvent Effects," Royaumont, France, edited by Y. Gauduel and P. J. Rossky (AIP, New York, 1994).

²(a) M. Cho, S. J. Rosenthal, N. F. Scherer, L. D. Ziegler, and G. R. Fleming, *J. Chem. Phys.* **96**, 5033 (1992); (b) R. Jimenez, G. R. Fleming, P. V. Kumar, and M. Maroncelli, *Nature* (London) **369**, 471 (1994); (c) R. S. Fee and M. Maroncelli, *Chem. Phys.* **183**, 235 (1994).

³M. Maroncelli and G. R. Fleming, *J. Chem. Phys.* **89**, 5044 (1988).

⁴M. Maroncelli, *J. Chem. Phys.* **94**, 2084 (1991).

⁵(a) T. Fonseca and B. M. Ladanyi, *J. Phys. Chem.* **95**, 2116 (1991); (b) T. Fonseca and B. M. Ladanyi, in Ref. 1(b), p. 380; (c) T. Fonseca and B. M.

Ladanyi, *J. Mol. Liq.* **60**, 1 (1994); (d) D. K. Phelps, M. J. Weaver, and B. M. Ladanyi, *Chem. Phys.* **176**, 575 (1993).

⁶E. A. Carter and J. T. Hynes, *J. Chem. Phys.* **94**, 5961 (1991).

⁷E. Neria and A. Nitzan, *J. Chem. Phys.* **96**, 5433 (1992).

⁸L. Perera and M. L. Berkowitz, *J. Chem. Phys.* **96**, 3092 (1992); **97**, 5253 (1992).

⁹(a) A. Chandra and B. Bagchi, *Chem. Phys.* **156**, 323 (1991); (b) S. Roy, S. Komath and B. Bagchi, *Proc. Ind. Acad. Sci. (Chemical Sciences)* **105**, 79 (1993); (c) S. Roy and B. Bagchi, *Chem. Phys.* **183**, 207 (1994), and more references to the work of this group therein.

¹⁰(a) F. O. Raineri, Y. Zhou, H. L. Friedman, and G. Stell, *Chem. Phys.* **152**, 201 (1991); (b) F. O. Raineri, H. Resat, and H. L. Friedman, *J. Chem. Phys.* **96**, 3068 (1992); (c) F. O. Raineri, H. Resat, B-Ching Perng, F. Hirata, and H. L. Friedman, *J. Chem. Phys.* **100**, 1477 (1994).

¹¹L. E. Fried and S. Mukamel, *J. Chem. Phys.* **93**, 932 (1990).

¹²M. Maroncelli, Vijaya P. Kumar, and A. Papazyan, *J. Phys. Chem.* **97**, 13 (1993).

¹³M. Maroncelli, P. V. Kumar, A. Papazyan, M. L. Horng, S. J. Rosenthal, and G. R. Fleming, in Ref. 1(b), p. 310.

¹⁴B. Bagchi, D. W. Oxtoby, and G. R. Fleming, *Chem. Phys.* **86**, 257 (1984).

¹⁵S. J. Rosenthal, R. Jimenez, G. R. Fleming, P. V. Kumar, and M. Maroncelli, *J. Mol. Liquids (Fonseca Memorial issue)* **60**, 25 (1994).

¹⁶E. Neria and A. Nitzan, *J. Chem. Phys.* **100**, 3855 (1994).

¹⁷D. Knödler, W. Dieterich, C. Lonsky, and A. Nitzan, *J. Chem. Phys.* **102**, 465 (1995).

¹⁸S.-Gang Su and J. D. Simon, *J. Phys. Chem.* **93**, 753 (1989).

¹⁹P. G. Wolynes, *J. Chem. Phys.* **86**, 5133 (1988).

²⁰I. Rips, J. Klafter, and J. Jortner, *J. Chem. Phys.* **88**, 3246; **89**, 4288 (1988).

²¹R. Richert, *Chem. Phys. Lett.* **199**, 355 (1992).

²²R. Richert and A. Wagener, *J. Phys. Chem.* **95**, 10115 (1991).

²³R. Richert, F. Stickel, R. S. Fee, and M. Maroncelli, *Chem. Phys. Lett.* (in press).

²⁴Y. J. Chang and E. W. Castner, *J. Chem. Phys.* **99**, 7289 (1993).

²⁵F. M. Gray, *Solid Polymer Electrolytes* (VCH, New York, 1991).

²⁶M. A. Ratner, in *Polymer Electrolyte Reviews*, edited by J. MacCallum and C. A. Vincent (Elsevier, New York, 1987), Vol. I, p. 173.

²⁷(a) L. M. Torell and S. Schantz, in *Polymer Electrolyte Reviews*, edited by J. MacCallum and C. A. Vincent (Elsevier, New York, 1988), Vol. II; (b) S. Schantz, L. M. Torell, and J. R. Stevens, *J. Chem. Phys.* **94**, 6862 (1991); (c) L. M. Torell, P. Jacobson, and G. Peterson, *Polymer Adv. Tech.* **4**, 152 (1993).

²⁸W. L. Jorgensen and J. Tirado-Rives, *J. Am. Chem. Soc.* **110**, 1657 (1988).

²⁹W. L. Jorgensen and M. Ibrahim, *J. Am. Chem. Soc.* **103**, 3976 (1981).

³⁰J. M. Briggs, T. Matsui, and W. L. Jorgensen, *J. Comput. Chem.* **11**, 958 (1990).

³¹S. J. Weiner, P. A. Kollman, D. A. Case, U. C. Singh, C. Ghio, G. Alagona, Jr., S. Profeta, and P. Weiner, *J. Am. Chem. Soc.* **106**, 765 (1984).

³²S. J. Weiner, P. A. Kollman, D. T. Nguyen, and D. A. Case, *J. Comput. Chem.* **7**, 230 (1986).

³³This truncation is not implemented for Coulomb terms between intramolecular charges because intramolecular distances are smaller than R_c and truncation will not affect them. In this case we use for definiteness a simple step function at R_c .

³⁴J. Chandrasekhar, D. C. Spellmeyer, and W. L. Jorgensen, *J. Am. Chem. Soc.* **106**, 903 (1984).

³⁵G. Allen, G. Gee, D. Mangaraj, D. Sims, and G. J. Wilson, *Polymer* **1**, 467 (1960).

³⁶H. C. Andersen, *J. Chem. Phys.* **72**, 2384 (1980).

³⁷J. W. de Leeuw, J. W. Perram, and E. R. Smith, *Annu. Rev. Phys. Chem.* **37**, 245 (1986).

³⁸The moments of inertia along the molecular principal axes are obtained by diagonalizing the moment of inertia tensor calculated for an "average" molecular configuration. For solvent I this configuration is obtained by using the average bond lengths and bond angles obtained from the simulation and a dihedral angle of 180° (the probability distribution for the dihedral angle shows a large peak at this angle and two smaller (by a factor of ~13) peaks at ±60°. These later structures are disregarded). For solvent II the "average configuration" is also constructed from averaged bond lengths and bond angles. In addition, dihedral angles of 180° for the C–O–C–C segments and 60° for the O–C–C–O segments are used. Similar principles are used for solvent III.

- ³⁹T. Shimanouchi, H. Matsuura, Y. Ogawa, and I. Harada, *J. Phys. Chem. Ref. Data* **7**, 1323 (1978).
- ⁴⁰See, for example, J. B. Hubbard and P. G. Wolynes, in *The Chemical Physics of Solvation*, edited by R. R. Dogonadze, E. Kalman, A. A. Kornyshev, and J. Ulstrup (Elsevier, Amsterdam, 1988), Vol. III, p. 33.
- ⁴¹See, for example, I. Ohmine and H. Tanaka, *Chem. Rev.* **93**, 2545 (1993).
- ⁴²E. Bart, A. Meltsin, and D. Huppert (unpublished).
- ⁴³M. Watanabe, T. T. Woster, and R. W. Murray, *J. Phys. Chem.* **95**, 4573 (1991).
- ⁴⁴P. Brus (unpublished).